Journal of Applied Sciences and Nanotechnology, Vol. 2, No. 3 (2022)

Journal of Applied Sciences and Nanotechnology

Journal homepage: https://jasn.uotechnology.edu.iq/

Preparation, Characterization and Mimetic Activities of Fe_2O_3 and Fe_3O_4 Nanoparticles as Catalase and Peroxidase

Alaa A. Majeed, Rashed T. Rasheed*

Applied Chemistry Division, Department of Applied Sciences, University of Technology – Iraq

Article information

Article history:
Received: January, 01, 2022
Accepted: March, 19, 2022
Available online: September, 10, 2022

Keywords:
Iron oxide,
Fe_3O_4,
Fe_2O_3,
Catalase,
Peroxidase,
Nanoparticles

Corresponding Author:
Rashed T. Rasheed
100010@uotechnology.edu.iq

Abstract

Different iron oxide nanoparticles (Fe_3O_4 and Fe_2O_3) were prepared by the sol-gel method (titration). The prepared nanoparticles were heated at 90 and 400°C. The morphology surface and structures were characterized by Fourier Transform Infra-Red (FT-IR) and Ultraviolet/Visible (Uv/Visible) measurements, X-ray diffraction (XRD), Scanning Electron Microscopy (SEM), and Atomic Force Microscope (AFM). The enzyme mimetic activities of these nanoparticles (Fe_3O_4 and Fe_2O_3) such as two enzymes (Catalase (CAT), and Peroxidase (Pxase)) were measured. The results showed the iron oxides (Fe_2O_3) heated at 90°C, have the maximum activity (189.99 $K.min^{-1}$) as catalase (CAT). While the iron oxides (Fe_3O_4) heated at 90°C, have the maximum activity (3.044 $U.min^{-1}$) as peroxidase (Pxase), and there is a decrease in the activity for both nanoparticles when annealed at 400°C. Despite the average grain size decrease in both samples, however, the mimetic activity decrease that is mean the average grain size is not affected in both mimetic activities as catalase and peroxidase.

DOI: 10.53293/jasn.2022.4574.1127, Department of Applied Sciences, University of Technology

1. Introduction

Nanostructures have attracted a significant amount of attention due to their better electrical, optical, magnetic, and physicochemical capabilities over their bulk counterparts because of their strong ferromagnetic characteristics [1], iron oxides have been frequently employed for a long time [2]. α-Fe_2O_3 is the best-studied polymorph found in nature as the mineral hematite. Hematite has a corundum-type rhombohedral hexagonal structure with a close-packed oxygen lattice in which two-thirds of the octahedral positions are filled by Fe (III) ions [3]. Ferrous ferric oxide, Fe_3O_4, often known as magnetite, is a well-crystallized type of iron oxide with significant magnetic characteristics that has been widely used in sensor fabrication, and considerable attention from researchers, especially for potential cancer detection and treatment [4, 5]. Because of their unique multifunctional capabilities, magnetic nanoparticles are top prospects for medicinal applications, [6, 7]. Iron oxide and its composites have been identified as interesting candidates for the removal of a wide range of pollutants, including organics, inorganic oxygen-containing groups, heavy metal cations, and heavy metal complex organics. Iron oxide has the added benefit of being a great visible light catalyser [8]. Because of their exceptional properties such as super magnetism, size, and the ability to obtain a compatible coating, iron oxide nanoparticles have greatly benefited medical applications such as magnetic resonance imaging (MRI), cell

separation and detection, tissue repair, magnetic hyperthermia, drug delivery, and therapy for apoptotic gene expression in tumors, and transfection of pro-BDNF into neural stem cells [9, 10]. Iron oxide lowers medication concentration, toxicity, and other negative consequences while increasing the efficacy of iron oxide-based treatment aside from its antibacterial effectiveness against a wide spectrum of pathogens, the toxicity of the iron oxide utilized to build the nanosystems is also addressed [11]. Nanozymes are a subset of nanoparticle-based catalysts that catalyze enzyme-like activities at room temperature nanozymes are intriguing not just because of their high stability and low cost, but also because they may be utilized to investigate fundamental processes at nanoscale surfaces [8]. Many nanoparticles, such as gold, graphene oxide, and other metal oxides, contain oxidase, peroxidase, and/or catalase-like activity. It's worth mentioning that, whereas many peroxidase nanozymes (those that employ H_2O_2 as a substrate) have been reported, only a few have oxidase activity [12]. Catalase (CAT) is an oxygen-consuming metalloprotein found in all organisms. Because this enzyme is soluble in erythrocytes and human erythrocytes are usually abundant in catalase, catalase activity in blood is almost entirely attributed to erythrocytes [13]. Peroxidase (Pxae) is a heme-containing enzyme that uses hydrogen peroxide to oxidize a variety of organic and inorganic compounds [14]. In this work, we prepared nano-oxides (Fe_2O_3 and Fe_3O_4) in the sol-gel method and measured their enzymatic activity (Catalase and peroxidase).

2. Experimental

2.1. Materials

Ammonium hydroxide (NH_4OH), iron (III) chloride $FeCl_3$, iron (II) sulfate $FeSO_4.7H_2O$) were purchased from Sigma (Sigma–Aldrich, Taufkirchen, Germany). Urea (NH_2CONH_2), dipotassium monohydrogen phosphate (K_2HPO_4), and potassium dihydrogen orthophosphate (KH_2PO_4**)** were purchased from (Merck, Germany), Cetyltrimethyl ammonium bromide (CTAP), and orthophenylene diamine (OPD) were purchased from (BDH-British), and hydrogen peroxide (H_2O_2) was purchased from (Chem-lab).

2.2. Preparation of iron oxide nanoparticles (Fe_2O_3 NPs)

Iron oxide (Fe_2O_3) nanoparticles were produced using a sol-gel technique, as described in the reference [15], with some modifications. This may be accomplished by using iron (III) chloride ($FeCl_3$), cetyltrimethylammonium bromide (CTAB), and ammonium hydroxide (NH_4OH) as described below. To begin, dissolve 3.0 gm. of $FeCl_3$ in distilled water. CTAB (0.5 gm.) in distilled water is dissolved and added to the $FeCl_3$ solution. Then, dilute the ammonium hydroxide in water (1:10) and begin titration until the reaction is complete (pH ≈ 8). The dark precipitate was washed more than 5 times in distilled water before being dried for 60 min at 90 °C. Then, it is annealed for 120 min at 400 °C. The reactions are explained by the equations:

$$\mathbf{FeCl_3 + 3NH_4OH \xrightarrow{CTAB} Fe(OH)_3 + 3NH_4Cl} \quad (1)$$

$$\mathbf{2Fe(OH)_3 \xrightarrow{400°C} Fe_2O_3 + 3H_2O} \quad (2)$$

2.3. Preparation of magnetite (Fe_3O_4) nanoparticles

Magnetite Fe_3O_4 nanoparticles were prepared using sol-gel methods as reference [16], with some modifications such as using a tight cover of parafilm to avoid oxidation and using $FeSO_4.7H_2O$, $FeCl_3$, CTAB, and NH_4OH, beginning with dissolving (0.695gm) of $FeSO_4.7H_2O$ in distilled water (40 ml). In addition to dissolving (0.41 gm) of $FeCl_3$ in distilled water and mixing it, dissolve (0.1 gm) of CTAB in distilled water and add to it. Then, dilute 10 mL of NH_4OH in 100 mL of distilled water and begin titration on the magnetic stirrer until the reaction is complete (pH ≈ 8). The black precipitate was rinsed with distilled water numerous times. The precipitate was then dried at 90 °C for 60 min then annealed at 400 °C for 120 min. The following equations explain the reactions:

$$\mathbf{FeCl_3+6NH_4OH \longrightarrow 2Fe2O_3+6NH_4Cl} \quad (3)$$

$$\mathbf{FeSO_4.7H_2O+2NH_4OH \longrightarrow FeO+(NH_4)2SO_4+7H_2O} \quad (4)$$

$$\mathbf{2FeCl_3+FeSO_4.7H_2O+8NH_4OH \xrightarrow{CTAB} [2Fe2O_3+FeO]+6NH_4Cl+(NH_4)2SO_4+7H_2O} \quad (5)$$

$$\mathbf{[2Fe2O_3+FeO] \xrightarrow{\Delta} Fe_3O_4+4H_2O} \quad (6)$$

2.4. Preparation of 50 mM phosphate buffer (pH =7.0)

The buffer solution was made by mixing the solutions listed below [17]:
Solution A: Dipotassium hydrogen orthophosphate anhydrous (50 mM). In a volumetric flask, dissolve (0.8710 gm) dipotassium monohydrogen phosphate (K_2HPO_4) in (10 ml.) of distilled water and then fill to (100 ml.).
Solution B: Potassium dihydrogen hydrogen orthophosphate anhydrous (KH_2PO_4) (50 mM). (0.6804 gm) of potassium dihydrogen orthophosphate (KH_2PO_4**)** was dissolved in (10 ml) of distilled water and filled a volumetric flask with (100 ml) of the solution. pH = 7.0 obtained by mixing (61.5 ml) of solution (A) with (38.5 ml) of solution (B).

3. Measuring enzymes

3.1. Measuring catalase (CAT) mimetic activity

Catalase (CAT) mimetic activity was measured using absorbance by the Uv/Visible spectrometer technique at a wavelength of 240 nm [18] as follows: three (50 mL) containers labeled (T, C, and B) for each nanoparticle (Fe_2O_3 and Fe_3O_4). Both the T and B containers received (0.001gm) and (0.002 gm) of (Fe_2O_3 and Fe_3O_4), respectively. In the C, B, and T containers, two and one milliliters of buffer phosphate (50 mM, pH = 7) were added, accordingly. T and C each received one milliliter of hydrogen peroxide (2.8 mM) containers. On the shaker, all containers were shaken for 5 min. The absorbance of each container is measured using a Uv/Visible spectrometer at a wavelength of 240 nm. Based on the first-order reaction, the following equation was utilized to calculate catalase mimetic activity [19].

$$\textbf{Catalase mimetic activity (K)} = \left(\frac{\mathbf{2.303}}{\mathbf{t}}\right)\mathbf{log}\left(\frac{\mathbf{Co}}{\mathbf{C}}\right) \tag{7}$$

Where, (t) denotes the response time in minutes. The concentrations of H_2O_2 in the cell reaction before and after the reaction is denoted by Co and C, respectively. C is the same as (C1 – T1).

3.2. Measuring peroxidase mimetic activity

The Uv/Visible spectrometer technique was used to assess the peroxidase mimetic activity of Fe_2O_3 and Fe_3O_4 at a wavelength of 292 nm as follows: three 50-mL containers labeled (T, C, and B) for each nanoparticle (Fe_2O_3 and Fe_3O_4). Both the T and B containers received a weight (0.012 gm) of (Fe_2O_3 and Fe_3O_4). T, C, and B containers received 4.95 mL and 5 mL of buffer phosphate (50 mM, pH = 7.2) accordingly. In the C and T containers, 0.05 ml of orthophenylene diamine (OPD) was added. Then, in each container, one milliliter of hydrogen peroxide (2.8 mM) was added. On the shaker, all containers were shaken for 5 min. The absorbance of each container is measured using a Uv/Visible spectrometer at a wavelength of 292 nm. The peroxidase mimetic activity was calculated using the equation below [20].

$$[\mathbf{C} - (\mathbf{T} - \mathbf{B})] = \frac{\mathbf{U}}{\mathbf{t}} \times \frac{(\mathbf{Vol} / \mathbf{Wt})}{\boldsymbol{t}} \tag{8}$$

Where B = blank, C = control, T = test, Vol = total volume of reaction solution, and Wt = weight of nanoparticles in container. t represents the response time after 45 min.

4. Results and Discussion

4.1. Optical Properties of the Nanoparticles Solutions

The optical characteristics of nanoparticle solutions were done by dissolving nanoparticles in ethanol (approximately 1×10^{-5} M), the optical properties (transmittance) were created of nanoparticles at different temperatures (90 and 400°C) ranging from 250 to about 550 nm.

4.1.1 The spectra of Fe_3O_4 Nanoparticles

The spectra of Fe_3O_4, Figure 1-a, show the transmittance edge is shifted to a higher wavelength (redshift) from 478 to 502 nm when increasing annealing temperature to 400 °C, resulting in higher optical transmittance and attributed to structural homogeneity and particle crystallization. The following equation can be used to calculate the value of the energy gap [21].

$$\textbf{Energy band gap (eV)} = \textbf{1240}/\boldsymbol{\lambda}\textbf{max} \quad (9)$$

Where 1240 is the factor used to convert nm to eV and λ_{max} is the maximum transmittance in nm. According to Eq. (9), the energy gap of Fe_3O_4 as-prepared is 2.59 eV, and that of annealing at 400 °C is 2.47 eV, this result agrees with the references [16, 17]

4.1.2. The spectra of Fe_2O_3 nanoparticles

The spectra of Fe_2O_3, Figure 1-b, illustrate the transmittance edge that has moved to a higher wavelength (redshift) from 476 to 492 nm with a rise in annealing temperatures to 400°C. As a result and Eq. (9) the energy gap of Fe_2O_3 as-prepared is 2.6 eV, while that of Fe_2O_3 annealing at 400°C is 2.52 eV this result agrees with the reference [22, 23].

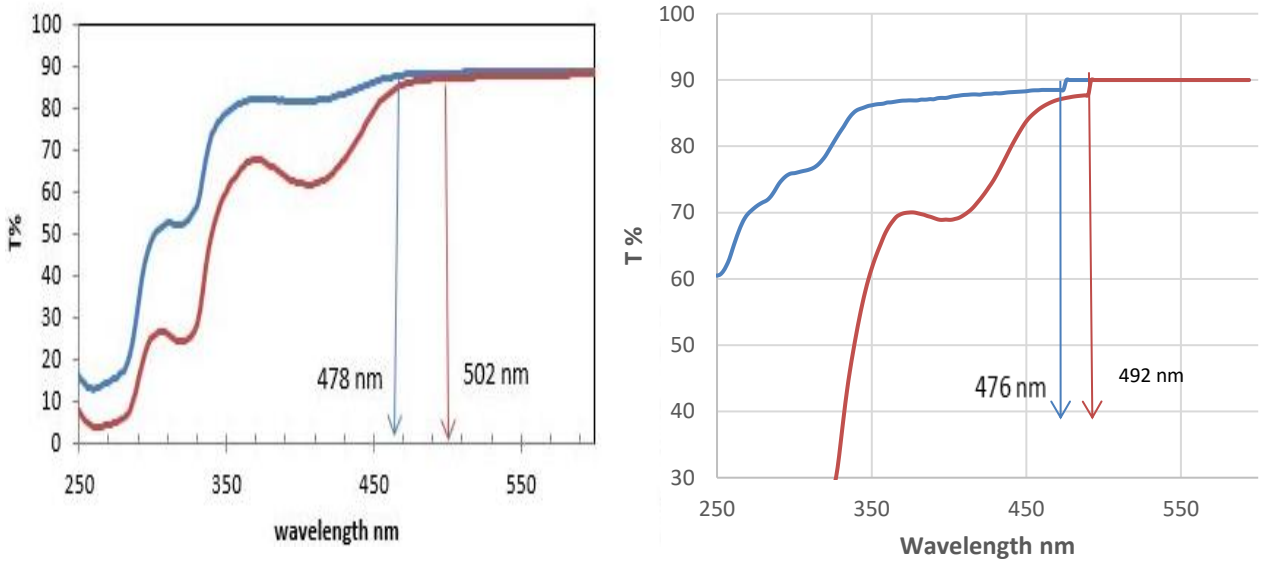

(a) **(b)**

Figure 1: The optical transmittance of (a) Fe_3O_4 NPs and (b), Fe_2O_3 NPs, as-prepared (blue line) and annealing at 400 °C (red line).

4.2. Fourier Transform Infrared Spectroscopy (FTIR)

The results of the Fourier Transform Infrared Spectroscopy (FTIR) tests disclose the absorption profile of the infrared spectra of nanoparticle samples. To describe these nanoparticles, an FTIR wavenumber range of 4000 to 400 cm^{-1} in the KBr disc was utilized.

4.2.1. FTIR spectra for Fe_3O_4 nanoparticles

Figure 2-a shows FTIR spectra for Fe_3O_4 as-prepared, the first two bands (3444 and 1629 cm^{-1}) are referred to as O-H bond vibrations stretching and bending of water, respectively, in iron hydroxide nanoparticles ($Fe(OH)_3$). These findings are consistent with the reference [24]. While the third band at 570 cm^{-1} is due to Fe-O vibration stretching [25]. In the spectrum of Fe_3O_4 nanoparticles (Figure 2-b), the stretching and bending vibrations of the O- H bond in water create two bands at 3440 and 1665 cm^{-1} respectively. The peaks at 532 and 445 cm^{-1} are caused by Fe-O vibrations. The results were quite similar to [26].

4.2.2. FTIR Spectra for Fe_2O_3 nanoparticles

Figure 2-c shows FTIR spectra for Fe_2O_3 as-prepared, with the shoulder at 3408 cm^{-1} and peak at 1629 cm^{-1} associated with OH stretching and bending, respectively. The two peaks of 474 and 437 cm^{-1} are attributable to Fe-O stretching vibrations; these results are similar to those reported in reference [27]. Figure 2-d shows an FTIR spectrum of samples annealed at 400 °C with four bands at 3420 and 1621 cm^{-1} corresponding to (O-H) bond stretching and bending vibrations of water. The vibrational modes (Fe-O) are seen at 451 and 534 cm^{-1} [11].

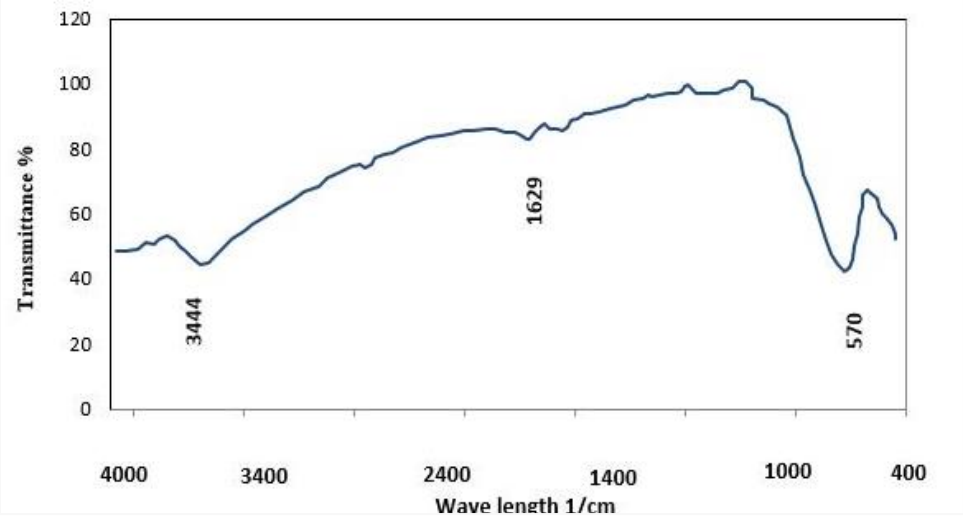
Transmittance %
120
100
80
60
40
20
0
3444
1629
570
4000
3400
2400
1400
1000
400
Wave length 1/cm

(a)

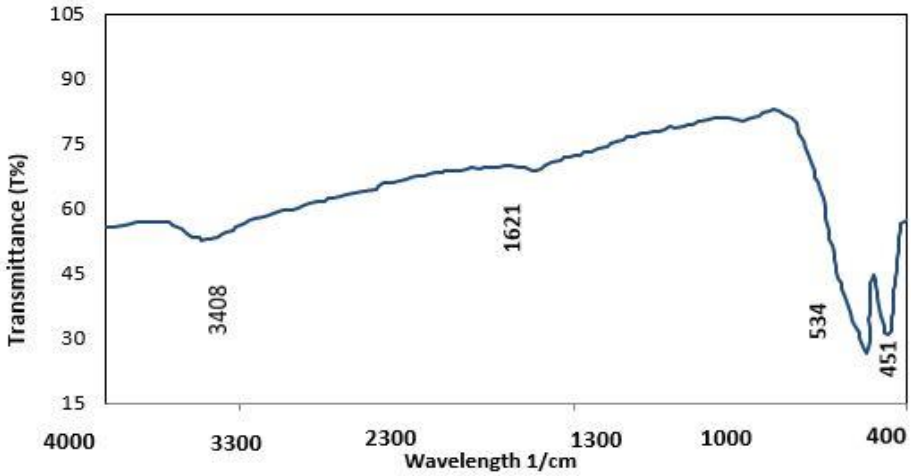
Transmittance (T%)
105
90
75
60
45
30
15
3408
1621
534
451
4000
3300
2300
1300
1000
400
Wavelength 1/cm

(b)

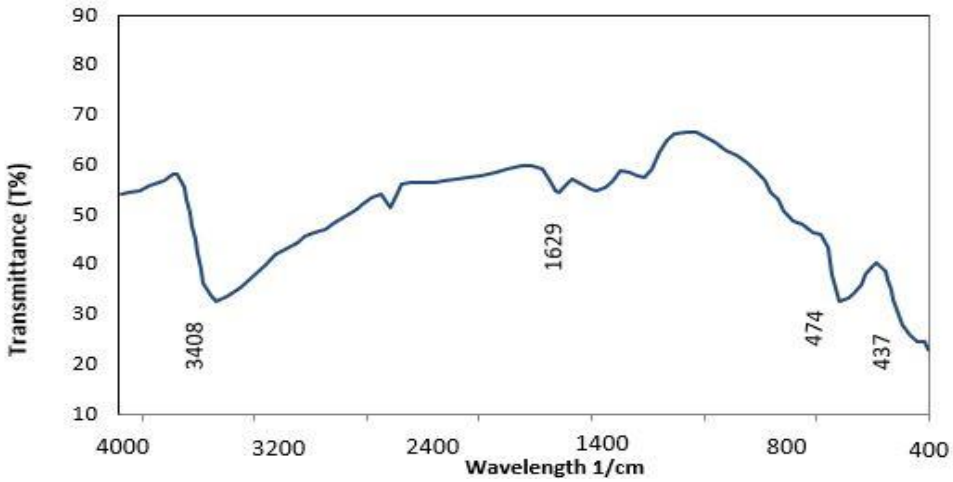
Transmittance (T%)
90
80
70
60
50
40
30
20
10
3408
1629
474
437
4000
3200
2400
1400
800
400
Wavelength 1/cm

(c)

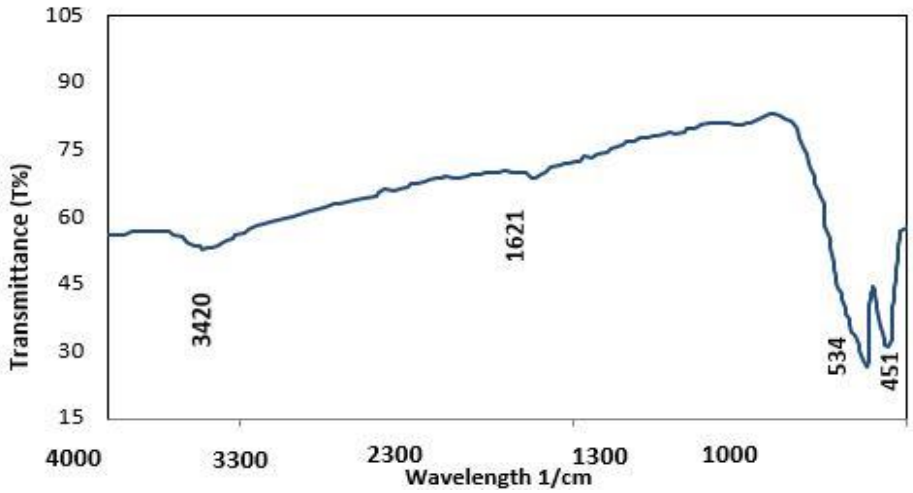

(d)

Figure 2: FTIR Spectra for Fe_3O_4 (a) as-prepared at 90°C for 60 min (b) annealing at 400 °C for 120 min, for Fe_2O_3 (c) as-prepared at 90°C for 60 min (d) annealing at 400 °C for 120 min.

4.3. X-Ray Diffraction (XRD)

4.3.1. The X-Ray Diffraction for Fe_3O_4 Nanoparticles

X-ray diffraction of magnetite nanoparticles (Fe_3O_4) as-prepared (Figure 3-a), indicated that magnetite is the primary component of this material, with additional phases of hematite (α-Fe_2O_3) and wustite (FeO). There are many peaks at (2θ = 24.06º, 33.11º, 49.45º, 54.04º, 62.49º, and 63.93º), for α-Fe_2O_3, (35.65º, 57.55º) for magnetite Fe_3O_4 [28], and (40.84 º) for FeO [29]. The XRD pattern of Fe_3O_4 nanoparticles follows the typical pattern in the JCPDS: (19-0629). When annealing at 400 ºC, (Figure 3-b, six distinct peaks (220), (311), (400) (422), (511) and (440) were detected at 2θ = 30.39º, 35.76º, 43.41º, 53.83º, 57.39º, and 62.97º respectively. Table 1 explains Fe_3O_4 at different temperatures, it demonstrates that the resulting particles are correct, emphasizing the spinel structure crystals of pure Fe_3O_4 of the nanoparticle [30]. The diffraction peaks might be attributed to a cubic structure of the Fe_3O_4 phase with the lattice value a = 8.39 °A [31].

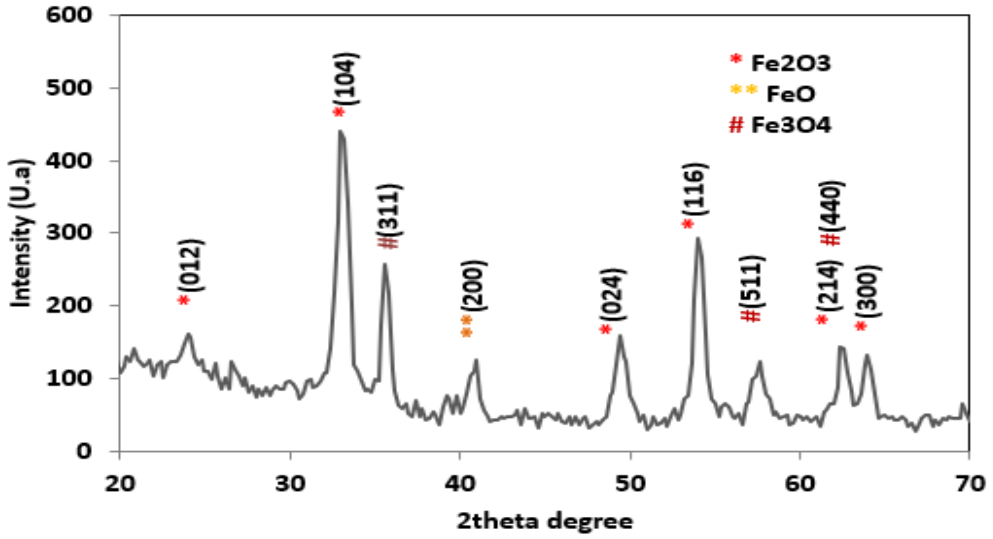

(a)

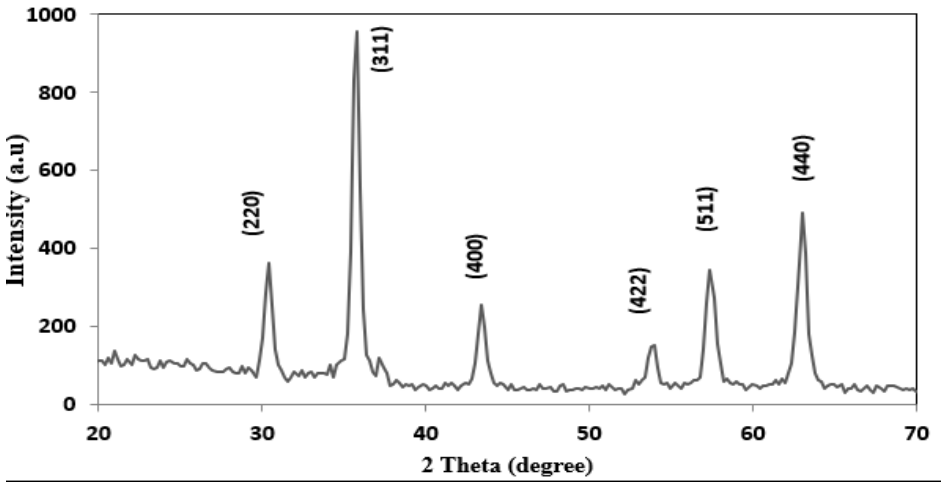

(b)

Figure 3: XRD of Fe_3O_4 (a) heating at 90 ºC for 60 min.(b) heating at 400 ◦C for 120 min.

The following is the Scherer's formula (Eq. (10)) for calculating the size of crystalline particles:

$$\mathbf{D = K\lambda/\beta \cos \theta} \tag{10}$$

Where K is a dimensionless quantity (≈ 0.94), (λ) is the X-ray wavelength, (β) is the line broadening at half-maximum intensity (FWHM), and (θ) is the Bragg angle [16]. According to Eq. (11), the lattice constants (a) of Fe_3O_4 nanoparticles were determined as in Table 1.

$$\mathbf{1/d^2 = (h^2 + K^2 + l^2)/a^2} \tag{11}$$

Where (d) is the interplanar distance, (hkl) Miller indices, and (a) is the Fe_3O_4 cubic structure's lattice constants [32].

Table 1: The result of the XRD for Fe_3O_4 at 90 ºC for 60 min, and 400 ºC for 120 min.

Nanoparticles	2θ (deg)	hkl	FWHM (deg)	d (A°)	D (A°)	Lattice constant a= b =c (A°)
Fe_3O_4 heating at 90 ◦C for 60 min	33.11	104	0.929	2.702	89.2	
	35.65	311	0.808	2.516	102.4	-
	54.04	116	0.871	1.695	103.2	-
Fe_3O_4 annealing at 400 ◦C for 120 min	35.76	311	0.641	2.50	130.1	8.39
	57.39	511	0.656	1.604	137.0	-
	62.97	440	0.641	1.474	145.4	-

4.3.2. The X-Ray Diffraction for Fe_2O_3 Nanoparticles

X-ray diffraction (XRD) of Fe_2O_3 was used as prepared measurements to verify the sample's crystal structure and phase composition. The indexed peaks and the recorded diffraction pattern are shown in Figure 4-a. There are three distinct peaks at 2θ = 26.94º, 35.35º, and 56.27º in the XRD pattern associated with the magnetite phase (211), (311) and (511) agree with this reference [33]. The XRD patterns obtained conform to the typical α-Fe_2O_3 pattern (JCPDS No. 33-0664; included in Figure 4-b. The unique peaks emerge at (2θ = 24.13°, 33.25°, 35.72°, 40.94°, 49.54°, 54.13°, 57.57°, 62.54°, and 64.06), which correspond to (012, 104, 110, 113, 024, 116, 018, 214, and 300) planes, respectively, and indicate its usual cubic spinel structure. This is consistent with the peculiar structure of pure α-Fe_2O_3 crystals, which have a rhombohedral centered hexagonal shape the maximum diffraction peak at 33.17° indicates that the prevalent α-Fe_2O_3 crystal structure has (104) faces [34]. The lattice

constants (a and c) of Fe_2O_3 nanoparticles were determined according to Eq. (12), as in Table 2.

$$1/d_{hkl}^2 = 4/3(h^2 + hk + k^2)/a^2 + l^2/c^2 \quad (12)$$

Where (d) is the interplanar distance, (hkl) are the Miller indices, and (a) and (c) is the lattice constants for the α-Fe_2O_3 hexagonal structure the computed the crystallite size (D) as well as the lattice constants (a and c) of Fe_2O_3[32]. The size of crystalline particles (D) can be calculated using the Shearer's equation (Eq. (10)).

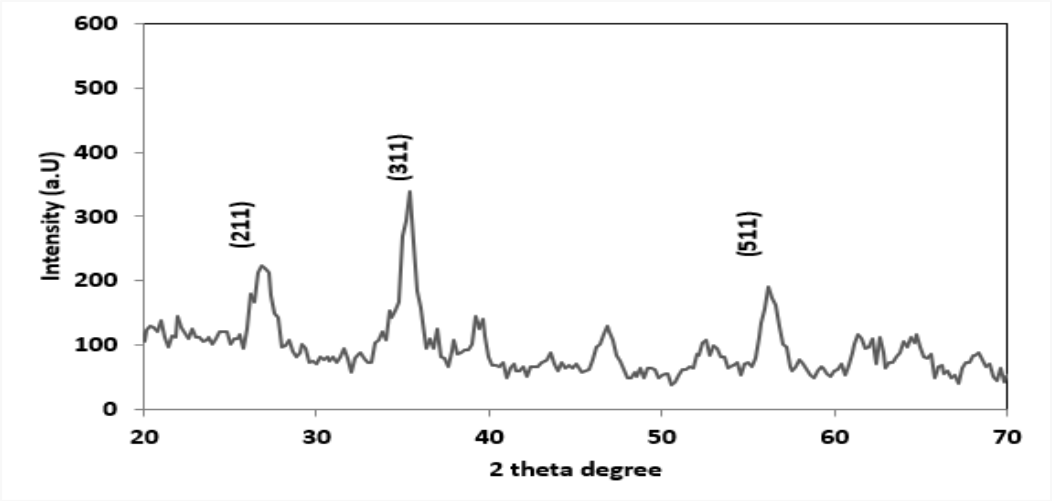

(a)

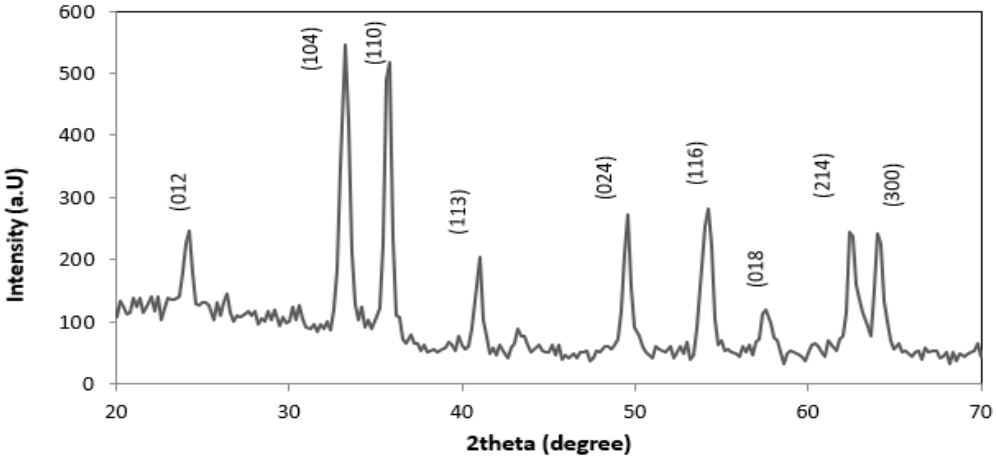

(b)

Figure 4: XRD of Fe_2O_3 (a) as prepared at 90 ºC for 60 min (b) heating at 400 ºC for 120 min.

Table 2: The result of the XRD for Fe_2O_3 at 90 ºC for 60 min, and at 400 ºC for 120 min.

Nanoparticles	2θ (deg)	hkl	FWHM (deg)	d (A°)	D (A°)	Lattice constant a = b (°A)	Lattice constant c (°A)
Fe_2O_3 heating at 60 ºC for 90 min	26.94	211	1.3270	3.3061	61.55		
	35.35	311	1.0450	2.537	83.71	-	-
	56.27	511	1.2277	1.633	73.30	-	-
Fe_2O_3 annealing at 400 ºC for 120 min	33.25	104	0.7733	2.692	107.2	5.02١	13.7٢١
	35.72	110	0.7809	2.511	106.9		
	54.13	116	0.7991	1.692	111.5	-	-

4.4. Surface Morphology by Scanning Electron Microscopy (SEM) and Energy Dispersive X-Ray Analysis (EDX).

The surface morphology image SEM with magnification at (100 K) and its EDX results of the metal oxides (Fe_3O_4 and Fe_2O_3) nanoparticles produced by hydrothermal technique and annealed to 400 °C for 120 min. It can be seen that Fe_3O_4 nanoparticles (Figure 5-a) have an irregular crystalline form, and the surface morphology analysis demonstrates the agglomeration of many ultrafine particles because of their small size seem as sawdust. While EDX results find the binding energies of O and Fe are shown as peaks in the Fe_3O_4 EDX spectrum (Figure 5-b) at 0.55, 0.7, 6.4, and 7.0 keV, respectively. The theoretical percentage calculations of Fe and O in the Fe_3O_4 nanoparticles are 42.85% and 57.14% respectively, while the experimental percentage calculations are 32.188% and 67.811% respectively. These results are listed in Table 3. About the SEM images of Fe_2O_3 nanoparticles show is irregularly assembled and agglomerated, very tiny in size, resembling fish eggs. (Figure 5-c). While EDX findings reveal that the binding energies of O and Fe are displayed as peaks in the Fe_2O_3 EDX spectrum (Figure 5-d) at 0.55, 0.7, 6.4, and 7.1 keV, respectively. Theoretical percentage estimates for Fe and O in Fe_2O_3 nanoparticles are 40% and 60%, respectively, while the experimental percentage calculations are 36.93% and 62.28% respectively, Table 3. Besides Cl and Si appearance in the EDX spectrum as process contaminations.

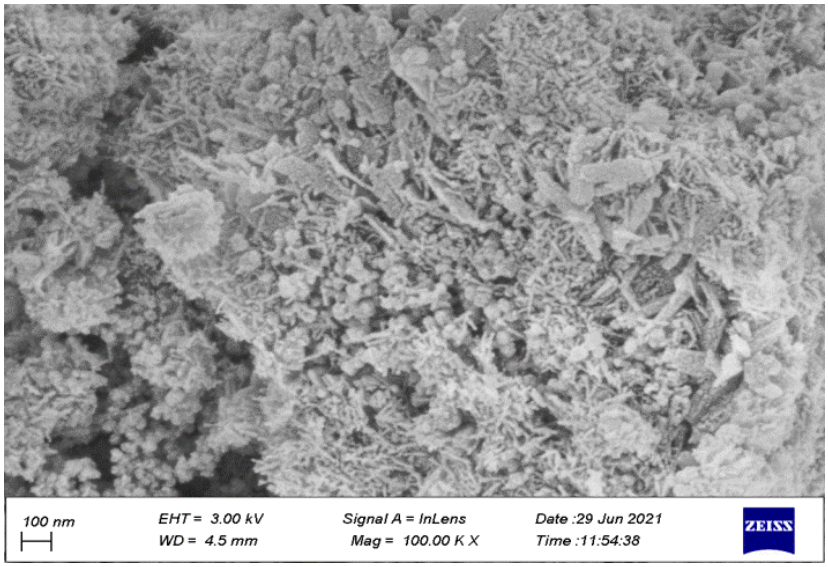

A

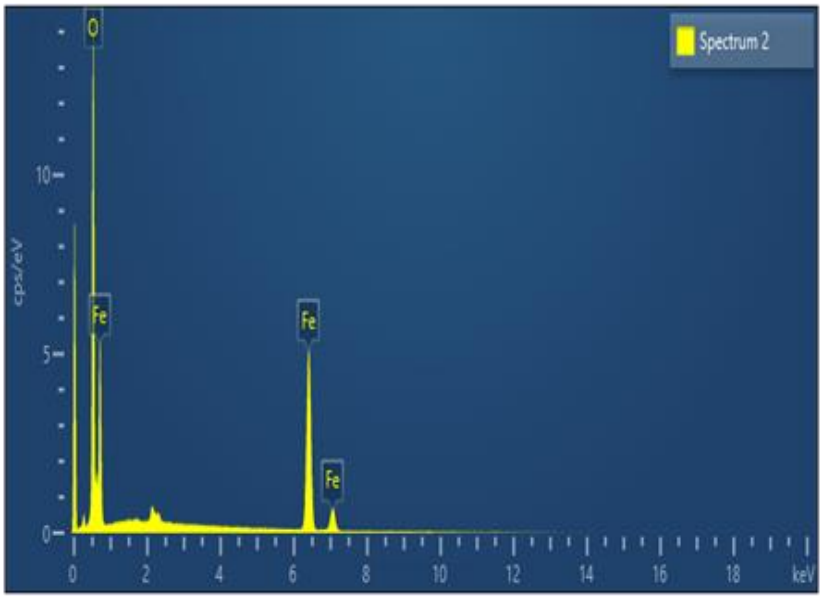

B

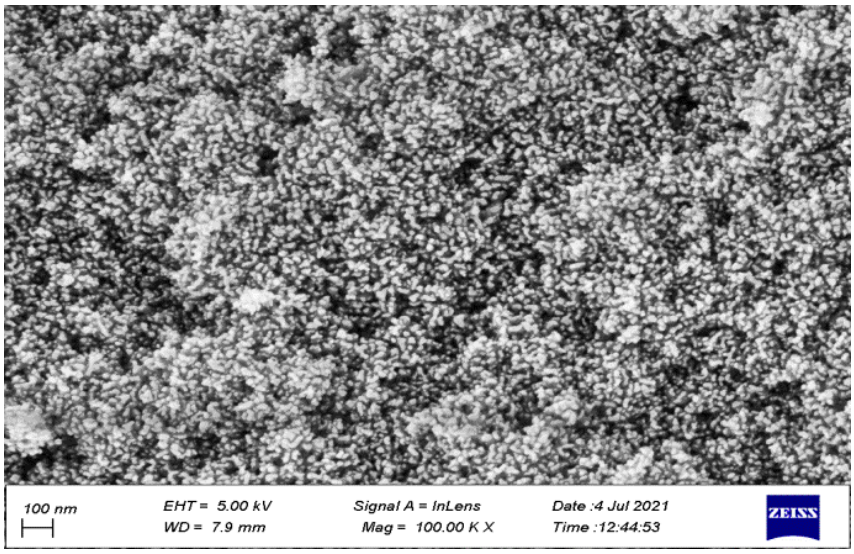

C

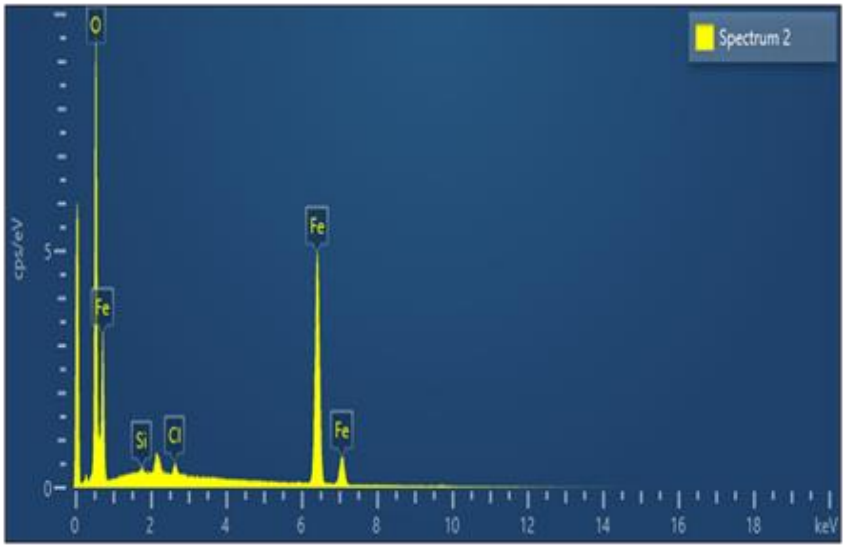

D

Figure 5: (a) SEM image and (b) EDX spectra of Fe_3O_4 and Fe_3O_4 respectively, (c) SEM image and (d) EDX spectrum Fe3O4.

Table 3: The elemental composition of Fe_3O_4 and Fe_2O_3 nanoparticles.

Nanoparticles	Element	Atomic Weight	Weight %	Theoretical %	Experimental %
Fe_3O_4	O	8	39.32	57.14	67.811
	Fe	26	60.68	42.85	32.188
	Total	-	100%	100%	100%
Fe_2O_3	O	8	33.87	60	62.28
	Fe	26	65.27	40	36.93
	Cl	17	0.62	-	0.53
	Si	14	0.24	-	0.25
Total	-	-	100%	100%	99.99%

4.5 Surface morphology

AFM results of nanoparticles (Fe_3O_4, Fe_2O_3) in three (3D) dimension images and Granularity accumulation distribution charts with different temperatures: (a) as-prepared (90 °C), and (b) 400 °C, as in Figure 6.

4.5.1. Iron oxide (Fe_3O_4) Nanoparticles

The distribution and accumulation of Fe_3O_4 nanoparticles convert from bubbles (Figure 7-a) to uniform shapes (Figure 7-b). This may relate to converting most of the hydroxides ($Fe(OH)_2$ and $Fe(OH)_3$) to oxides form (Fe_3O_4) when heating at a high temperature (400 °C). The average grain size decreases from 91.36 nm (as-prepared) to 69.44 nm (annealing), as in Table 4, the decrease in the size may be due to converting the sample from hydroxide to oxide as the Eq. (6).

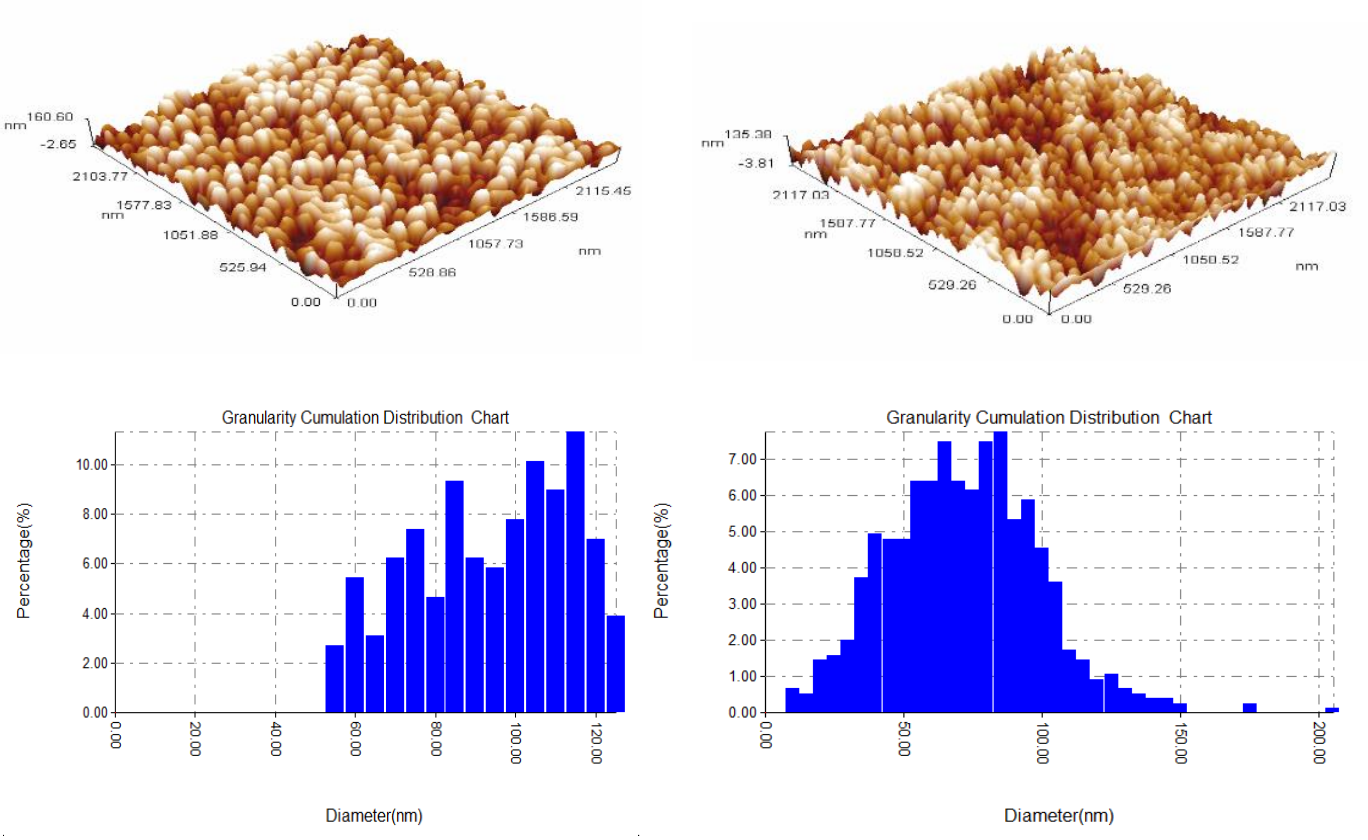

A B

Figure 6: AFM images at 3D and Granularity accumulation distribution charts of Fe_3O_4 (a) as-prepared and (b) annealing, and Fe_2O_3 at 400 °C for 120 min respectively.

4.5.2. Iron oxide (Fe_2O_3) Nanoparticles

The distribution and accumulation of Fe_2O_3 nanoparticles convert from random shapes (Figure7-c) into more regular shapes (Figure 7-d). This relates to converting most of the hydroxides ($Fe(OH)_3$) to oxides (Fe_2O_3) when heating at a high temperature (400 °C). While the average grain size increases from 104.52 nm (as-prepared) to 90.25 nm (annealing), as in Table 5, the increase in the size may be due to the accumulation of the nanoparticles of the sample as the Eq. (2).

Table 5: Average grain size of (Fe_3O_4 and Fe_2O_3) nanoparticles heating at (90 and 400 °C).

Nanoparticles	**Average grain size(d) (nm) heating at**	
	90 °C	**400 °C**
Fe_3O_4	91.36 nm	69.44 nm
Fe_2O_3	104.52 nm	90.25 nm

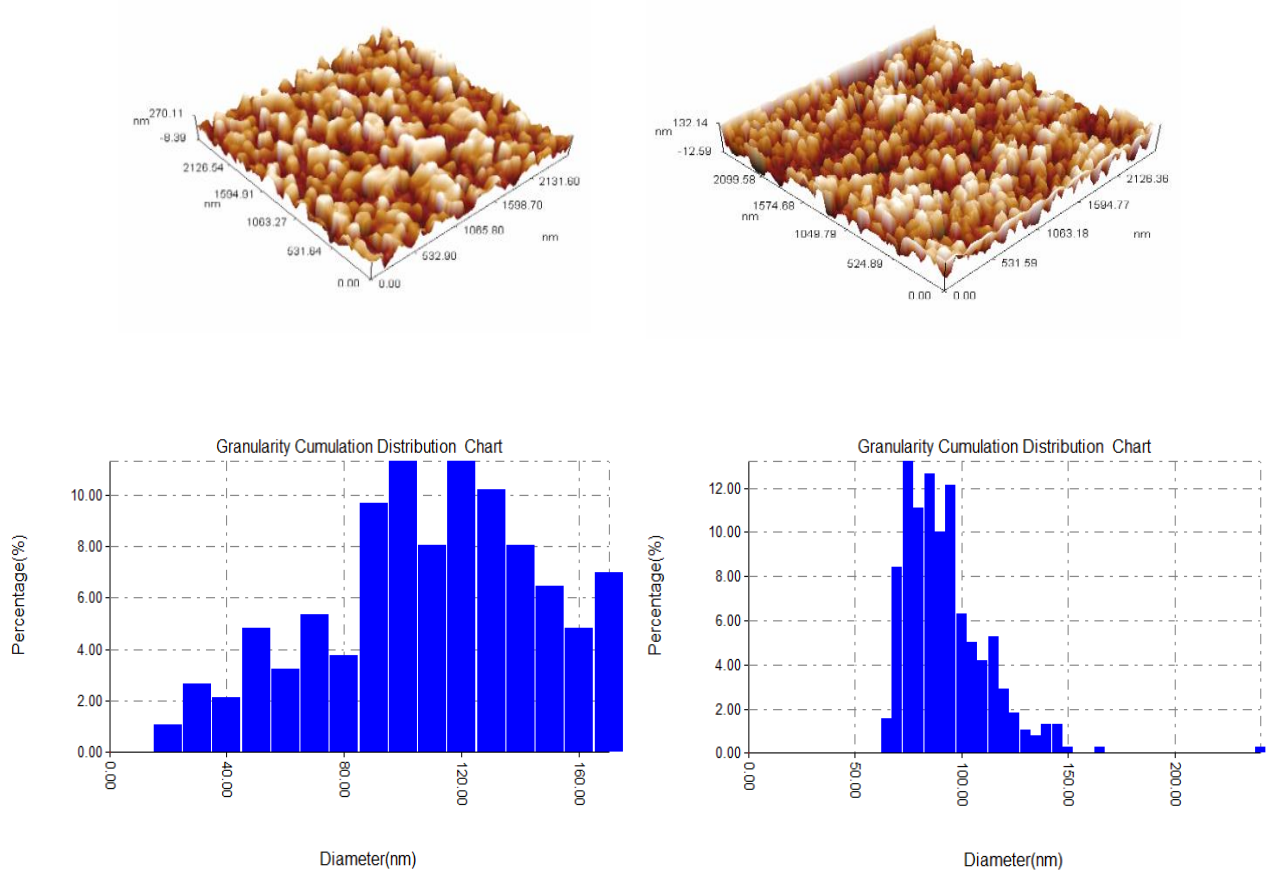

C D

Figure 6: AFM images at 3D and Granularity accumulation distribution charts of Fe_3O_4 (c) as-prepared and (d) annealing at 400 °C for 120 min respectively.

5. Applications

5.1. Catalase Mimetic Activity

The mimetic activities of our prepared nanoparticles as catalase (CAT) in phosphate buffer solution (50 mM, pH= 7), using spectrophotometric method [19], at the wavelength (λ = 240 nm), The CAT mimetic activity was determined by the Eq. (7). The results show the CAT mimetic activities of the nanoparticles are different according to their types and the degree of heating temperatures. The highest CAT mimetic activity of the nanoparticles (as-prepared) relates to Fe_2O_3 while the lowest activity relates to Fe_3O_4.

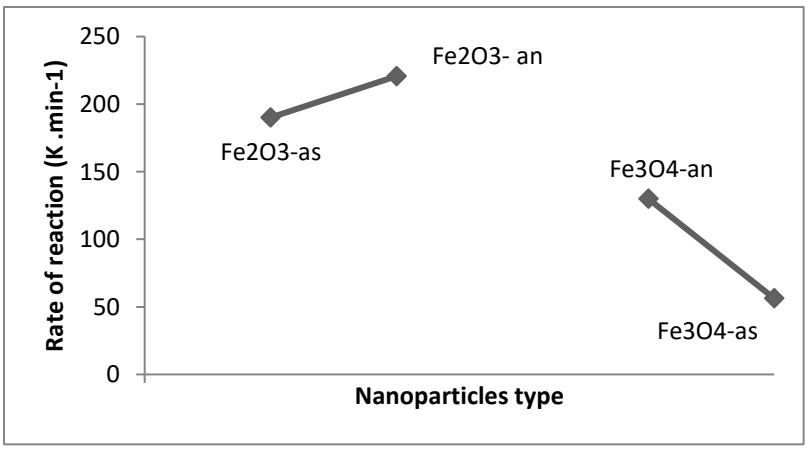

Figure 7: CAT mimetic activity curve of nanoparticles at two temperatures (90 and 400 °C).

Also, the highest CAT mimetic activity of the nanoparticles (annealing) relates to Fe_2O_3 while the lowest activity relates to Fe_3O_4, as in Figure 7 and Table 6. The increased CAT mimetic activity of Fe_2O_3, when annealing at 400 °C, may be due to converting the sample from a nonmagnetic to a magnetic form. Meanwhile, the high decrease in CAT mimetic activity of Fe_3O_4 (annealing) compared with its as-prepared (from 129.89 K. min^{-1} to 56.20 K. min^{-1}), may be related to losing its magnetic property.

Table 6: CAT mimetic activity values of nanoparticles at two temperatures (90 °C and 400 °C).

Metal Oxide Nanoparticles	CAT activity (K. min^{-1})	
	As-prepared	Annealing
Fe_3O_4	129.89	56.20
Fe_2O_3	189.99	220.71

5.2. Peroxidase Mimetic Activity

The mimetic activities of our nanoparticles (Fe_3O_4 and Fe_2O_3) as peroxidase (Pxase) in phosphate buffer solution (50 mM, pH= 7.2), utilizing the reference [20], with some modification by employing spectrophotometric technique at a wavelength (λ = 292 nm), including the use of orthophenylenediamine solution as an indicator, The equation was used to calculate the peroxidase mimetic activity (8). The results show the Pxase mimetic activities of nanoparticles were depending on the kind of nanoparticle and the degree of heating. The nanoparticles with the highest Pxase mimetic activities (as prepared) are Fe_3O_4, while the nanoparticles with the lowest activity are Fe_2O_3. The nanoparticles with the highest Pxase mimetic activities (annealing at 400 °C) are Fe_2O_3, while the nanoparticles with the lowest activity are Fe_3O_4. The simulation activity was arranged in the following order (Fe_2O_3> Fe_3O_4) exactly the opposite of the as-prepared, as shown in Figure 8 and Table 7. The high decrease in Pxase mimetic activity of Fe_3O_4 compared with its as-prepared (from 3.044 U/min^{-1} to 0.640 U/min^{-1}), may be related to losing its magnetic property when annealing at 400 °C. While the increased the Pxase mimetic activity of Fe_2O_3 (as-prepared) nonmagnetic sample ($Fe(OH)_3$) more than the magnetic sample (Fe_2O_3) when annealing at 400 °C, despite the average grain size of as-prepared is larger than annealing samples (104.52 to 90.25 nm) respectively, Table 7 this indicates that the average grain size does not affect in Pxase mimetic activity. Despite the decrease in the average grain size in all annealing samples, there are no effects on Pxase mimetic activity.

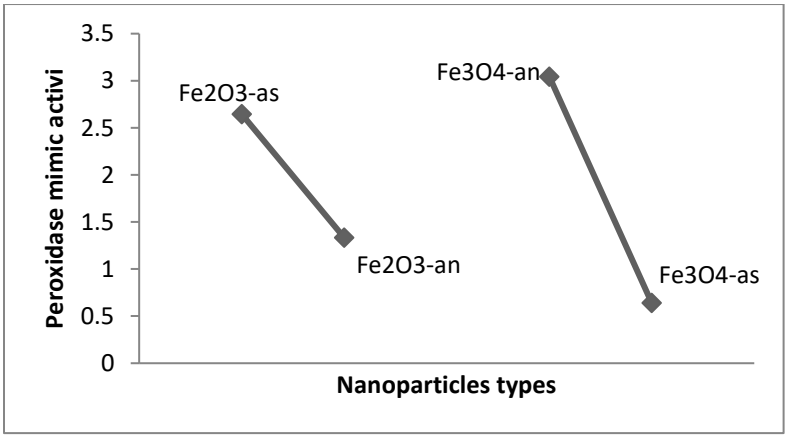

Figure 8: Peroxidase the mimetic activity of nanoparticles at two temperatures (90 and 400 °C).

Table 7: Peroxidase mimetic activities of metal oxides nanoparticles heating at 90 °C for 60 min and annealing at 400 °C for 120 min

Metal Oxide Nanoparticles	Peroxidase activity (U/min^{-1})	
	As-prepared	Annealing
Fe_3O_4	3.044	0.640
Fe_2O_3	2.644	1.333

6. Conclusions

Iron oxides nanoparticles (Fe_3O_4 and Fe_2O_3) have been successfully synthesized by the Sol-Gel. Both nanoparticles were heated at two temperatures (90 and 400 ^oC), then characterized by different techniques such as FT-IR, Uv/Visible, XRD, SEM, and AFM. The AFM study showed that the grain size of the powders annealing at 400 ^oC, was 90.25 and 69.44 nm for Fe_3O_4 and Fe_2O_3 respectively. Catalase (CAT) and peroxidase (Pxase) mimetic activities were measured against H_2O_2 and OPD as substrate respectively. The results indicated that the highest mimetic activities as CAT for Fe_3O_4 were at sample heated at 90 ^oC, while that for Fe_2O_3 were at same annealing at 400 ^oC because both samples have magnetite properties. On the other hand, the mimetic activities as Pxase of iron oxides nanoparticles were found when heated at 90 ^oC, compared with corresponding their iron oxides heated at 400 ^oC. Despite the average grain size was decreased with heating in both samples. This means the particle size of these nanoparticles does not affect the mimetic activity of CAT and Pxase.

Acknowledgment

We are thankful for the University Technology/ Applied Sciences Department / Applied Chemistry Division Laps and all laboratory staff who assisted us in the measurements.

Conflict of Interest

There are no conflicts of interest.

References

[1] A. Lassoued, M. S. Lassoued, B. Dkhil, S. Ammar, and A. Gadri, “Synthesis, photoluminescence and Magnetic properties of iron oxide (α-Fe_2O_3) nanoparticles through precipitation or hydrothermal methods,” Physica E: Low-Dimensional Systems and Nanostructures, vol. 101, p. 212–219, 2018, doi: 10.1016/j.physe.2018.04.009.

[2] X. M. Liu, S. Y. Fu, H. M. Xiao, and C. J. Huang, “Preparation and characterization of shuttle-like α-Fe_2O_3 nanoparticles by supermolecular template,” Journal of Solid State Chemistry, vol. 178(9), p. 2798–2803, 2005, doi: 10.1016/j.jssc.2005.06.018.

[3] R. Zboril, M. Mashlan, and D. Petridis, “Iron(III) oxides from thermal processes-synthesis, structural and magnetic properties, Mössbauer spectroscopy characterization, and applications,” Chemistry of Materials, vol. 14(3), p. 969–982, 2002, doi: 10.1021/cm0111074.

[4] M. Jouyandeh, S. M. R. Paran, M. Shabanian, S. Ghiyasi, H. Vahabi, M. Badawi, F. Krzyszt, P. Debora, and R. S. Mohammad, “Curing behavior of epoxy/Fe_3O_4 nanocomposites: A comparison between the effects of bare Fe_3O_4, Fe_3O_4/SiO_2/chitosan and Fe_3O_4/SiO_2/chitosan/imide/phenylalanine-modified nanofillers,” Progress in Organic Coatings, vol. 123, p. 10–19, 2018, doi: 10.1016/j.porgcoat.2018.06.006.

[5] S. Albukhaty, S. Al-Musawi, S. Abdul Mahdi, G. M. Sulaiman, M. S.Alwahibi, Y. H.Dewir,and H. Rizwana. "Investigation of Dextran-Coated Superparamagnetic Nanoparticles for Targeted Vinblastine Controlled Release, Delivery, Apoptosis Induction, and Gene Expression in Pancreatic Cancer Cells", Molecules, vol. 25(20), p. 4721.2020. doi:10.3390/molecules25204721

[6] S. Upadhyay, K. Parekh, and B. Pandey, “Influence of crystallite size on the magnetic properties of Fe3O4 nanoparticles,” Journal of Alloys and Compounds, vol. 678, p. 478–485, 2016, doi: 10.1016/j.jallcom.2016.03.279.

[7] S. Al-Musawi, S.Ibraheem, S.Abdul Mahdi, S.Albukhaty, A. J.Haider, A. A.Kadhim, and H.Al-Karagoly,“Smart Nanoformulation Based on Polymeric Magnetic Nanoparticles and Vincristine Drug: A Novel Therapy for Apoptotic Gene Expression in Tumors”. Life, vol. 11(1), p. 71, 2021. doi:10.3390/life11010071.

[8] H. Tao, Qingqing Bi, Jingtao Huang, Xin Wei, Rongli Wang, Ting Zhou, and Yanan Hao, “Fabrication, application, optimization and working mechanism of Fe_2O_3 and its composites for contaminants elimination from wastewater,” Chemosphere, vol. 263, p. 127889, 2021.doi: 10.1016/j.chemosphere.2020.127889.

[9] L. S. Arias, J. P. Pessan, A. P. M. Vieira, T. M. T. de Lima, A. C. B. Delbem, and D. R. Monteiro, “Iron oxide nanoparticles for biomedical applications: a perspective on synthesis, drugs, antimicrobial activity, and toxicity,” Antibiotics, vol. 7(2), p. 46, 2018. doi: 10.3390/antibiotics7020046.

[10] S. N. Albukhaty, H. Naderi-Manesh, T. Taqi, and M. Sakhi Jabir,“Poly-l-lysine-coated superparamagnetic nanoparticles: a novel method for the transfection of pro-BDNF into neural stem cells. Artificial Cells”, Nanomedicine, and Biotechnology, p. 1–8, 2018. doi:10.1080/21691401.2018.1489272

[11] R. T. Rasheed, S. D. Al-Algawi, H. H. Kareem, and H. S. Mansoor, "Preparation and characterization of hematite iron oxide (α-Fe_2O_3) by sol-gel method," Chem Sci J, vol. 9(197), p. 2, 2018. doi: 10.4172/2150-3494.1000197.
[12] B. Liu, Z. Huang, and J. Liu, "Boosting the oxidase mimicking activity of nanoceria by fluoride capping: Rivaling protein enzymes and ultrasensitive F- detection," Nanoscale, vol. 8(28), p. 13562–13567, 2016, doi: 10.1039/c6nr02730j.
[13] I. Fridovich and B. Freeman, "Antioxidant defenses in the lung," Annual review of physiology, vol. 48(1), p. 693–702, 1986. doi:10.1146/annurev.ph.48.030186.003401.
[14] N. C. Veitch, "Horseradish peroxidase: A modern view of a classic enzyme," Phytochemistry, vol. 65(3), p. 249–259, 2004, doi: 10.1016/j.phytochem.2003.10.022.
[15] Raja, K Jaculine, M Mary Jose, M Verma, Sunil Prince, A A M Ilangovan, K Sethusankar, K Das, and S Jerome., "Sol–gel synthesis and characterization of α-Fe_2O_3 nanoparticles," Superlattices and Microstructures, vol. 86, p. 306–312, 2015. doi.org/10.1016/j.spmi.2015.07.044.
[16] Z. I. Takai, M. K. Mustafa, S. Asman, and K. A. Sekak, "Preparation and characterization of magnetite (Fe_3O_4) nanoparticles by sol-gel method," Int. J. Nanoelectron. Mater, vol. 12, p. 37–46, 2019.
[17] H. Aebi, "Catalase," in Methods of enzymatic analysis, Elsevier, 1974, p. 673–684.
[18] R. T.Rasheed, , H. S.Mansoor, and A. S.Mansoor, New colorimetric method to determine catalase mimic activity. Materials Research Express, vol. 7(2), 025405, 2020. doi:10.1088/2053-1591/ab706b .
[19] R. F. Beers and I. W. Sizer, "A spectrophotometric method for measuring the breakdown of hydrogen peroxide by catalase," Journal of biological chemistry, vol. 195(1), p. 133–140, 1952.
[20] S. Fornera and P. Walde, "Spectrophotometric quantification of horseradish peroxidase with o-phenylenediamine," Analytical Biochemistry, vol. 40792), p. 293–295, 2010, doi: 10.1016/j.ab.2010.07.034.
[21] Y. P.Yew, K.Shameli, M.Miyake, N.Kuwano, N. B. Bt Ahmad Khairudin, S. E. Bt Mohamad, and K. X.Lee, Green Synthesis of Magnetite (Fe3O4) Nanoparticles Using Seaweed (Kappaphycus alvarezii) Extract. Nanoscale Research Letters, 11(1), 2016. doi:10.1186/s11671-016-1498-2
[22] H. El Ghandoor , H. M. Zidan , Mostafa M.H. Khalil and M. I. M. Ismail "Synthesis and Some Physical Properties of Magnetite (Fe3O4) Nanoparticles." Int. J. Electrochem. Sci., 7, p. 5734 - 5745. 2012
[23] A. J. Deotale and R. V Nandedkar, "ScienceDirect Correlation between Particle Size , Strain and Band Gap of Iron Oxide Nanoparticles," Materials Today: Proceedings, vol. 3(6), p. 2069–2076, 2016, doi: 10.1016/j.matpr.2016.04.110.
[24] A. H. M. Yusoff, M. N. Salimi, and M. F. Jamlos, "Synthesis and characterization of biocompatible Fe3O4 nanoparticles at different pH," AIP Conference Proceedings, vol. 1835, p. 1–5, 2017, doi: 10.1063/1.4981832.
[25] W. Lu, Y. Shen, A. Xie, and W. Zhang, "Green synthesis and characterization of superparamagnetic Fe3O4 nanoparticles," Journal of Magnetism and Magnetic Materials, vol. 322(13), p. 1828–1833, 2010, doi: 10.1016/j.jmmm.2009.12.035.
[26] A. Jafari, S. F. Shayesteh, M. Salouti, and K. Boustani, "Effect of annealing temperature on magnetic phase transition in Fe3O4 nanoparticles," Journal of Magnetism and Magnetic Materials, vol. 379, p. 305–312, 2015.
[27] F. Li, X. Wang, H. Pan, Q. Li, and J. Yang, "Preparation of disk-like A-Fe2O3 nanoparticles and their catalytic effect on extra heavy crude oil upgrading," Fuel, vol. 251, p. 644–650, 2019, doi: 10.1016/j.fuel.2019.04.048.
[28] V. E. Noval and C. Universitaria, "Fe_3O_4 -TiO_2 and Fe_3O_4 -SiO_2 Core-shell Powders Synthesized from Industrially Processed Magnetite (Fe_3O_4) Microparticles," vol. 22(3), 2019. doi:10.1590/1980-5373-mr-2018-0660.
[29] X. Zhang, Y. Niu, X. Meng, Y. Li, and J. Zhao, "Structural evolution and characteristics of the phase transformations between α-Fe_2O_3, Fe_3O_4 and γ-Fe_2O_3 nanoparticles under reducing and oxidizing atmospheres," Cryst.Eng.Comm, vol. 15(40), p. 8166–8172, 2013. doi:10.1039/c3ce41269e.
[30] N. Yadav, R. K. Jarial, and U. M. Rao, "Characterization of mineral oil based Fe3O4 nanofluid for application in oil filled transformers," International Journal on Electrical Engineering and Informatics, vol. 10(2), p. 338–349, 2018, doi: 10.15676/ijeei.2018.10.2.10.
[31] S. H. Chaki, T. J. Malek, M. D. Chaudhary, J. P. Tailor, and M. P. Deshpande, "Magnetite Fe_3O_4 nanoparticles synthesis by wet chemical reduction and their characterization," Advances in Natural Sciences: Nanoscience and Nanotechnology, vol. 6(3), p. 35009, 2015.

[32] W. A. Wooster, Crystal structure, vol. 236, P. 5345. 1972.
[33] A. Ruíz-baltazar, R. Esparza, G. Rosas, and R. Pérez, "Effect of the Surfactant on the Growth and Oxidation of Iron Nanoparticles Effect of the Surfactant on the Growth and Oxidation of Iron Nanoparticles,"vol. 2015, p. 1-8, 2015, doi: 10.1155/2015/240948.
[31] Karade, V C Parit, S B Dawkar, V V Devan, R S Choudhary, R J Kedge, V V Pawar, N V Kim, J H Chougale, and A D., "Heliyon A green approach for the synthesis of α -Fe_2O_3 nanoparticles from Gardenia resinifera plant and it ' s In vitro hyperthermia application," Heliyon, vol. 5, p. e02044, 2019, doi: 10.1016/j.heliyon.2019.e02044.
[34] S. Elbasuney, G. S. El-sayyad, A. A. Elmotaz, M. A. Sadek, and H. Tantawy, "signature via synergism of nanothermite and reduced graphene oxide Multi-component nanocomposite infrared flare with superior infrared signature via synergism of nanothermite and reduced graphene oxide," Journal of Materials Science: Materials in Electronics, 2020, doi: 10.1007/s10854-020-03699-8.